



Article

Green Synthesis of CeO₂ Nanoparticles from the *Abelmoschus esculentus* Extract: Evaluation of Antioxidant, Anticancer, Antibacterial, and Wound-Healing Activities

Hafiz Ejaz Ahmed ¹, Yasir Iqbal ², Muhammad Hammad Aziz ^{2,*}, Muhammad Atif ³, Zahida Batool ¹, Atif Hanif ⁴, Nafeesah Yaqub ³, W. A. Farooq ³, Shafiq Ahmad ⁵, Amanullah Fatehmulla ³ and Hijaz Ahmad ⁶

¹ Institute of Physics: The Islamia University of Bahawalpur, Bahawalpur 63100, Pakistan; mejaz.ahmed@iub.edu.pk (H.E.A.); zahida.batool@iub.edu.pk (Z.B.)

² Department of Physics, COMSATS University Islamabad, Lahore 54000, Pakistan; yasiriqbal485@gmail.com

³ Department of Physics and Astronomy, College of Science, King Saud University, P.O. Box 2455, Riyadh 11451, Saudi Arabia; muhatif@ksu.edu.sa (M.A.); 437203488@ksu.edu.sa (N.Y.); wafarooq@hotmail.com (W.A.F.); aman@ksu.edu.sa (A.F.)

⁴ Botany and Microbiology Department, College of Science, King Saud University, Riyadh 11451, Saudi Arabia; ahchaudhry@ksu.edu.sa

⁵ Industrial Engineering Department, College of Engineering, King Saud University, P.O. Box 800, Riyadh 11421, Saudi Arabia; ashafiq@ksu.edu.sa

⁶ Section of Mathematics, International Telematic University Uninettuno, Corso Vittorio Emanuele II, 39, 00186 Roma, Italy; hijaz555@gmail.com

* Correspondence: hammadaziz@cuilahore.edu.pk; Tel.: +308-7535035



Citation: Ahmed, H.E.; Iqbal, Y.; Aziz, M.H.; Atif, M.; Batool, Z.; Hanif, A.; Yaqub, N.; Farooq, W.A.; Ahmad, S.; Fatehmulla, A.; et al. Green Synthesis of CeO₂ Nanoparticles from the *Abelmoschus esculentus* Extract: Evaluation of Antioxidant, Anticancer, Antibacterial, and Wound-Healing Activities. *Molecules* **2021**, *26*, 4659. <https://doi.org/10.3390/molecules26154659>

Academic Editors: Kok Hwa Lim and Antonio Zuorro

Received: 9 June 2021

Accepted: 26 July 2021

Published: 31 July 2021

Publisher's Note: MDPI stays neutral with regard to jurisdictional claims in published maps and institutional affiliations.



Copyright: © 2021 by the authors. Licensee MDPI, Basel, Switzerland. This article is an open access article distributed under the terms and conditions of the Creative Commons Attribution (CC BY) license (<https://creativecommons.org/licenses/by/4.0/>).

Abstract: Metal oxide nanoparticles synthesized by the biological method represent the most recent research in nanotechnology. This study reports the rapid and ecofriendly approach for the synthesis of CeO₂ nanoparticles mediated using the *Abelmoschus esculentus* extract. The medicinal plant extract acts as both a reducing and stabilizing agent. The characterization of CeO₂ NPs was performed by scanning electron microscopy (SEM), X-ray diffraction (XRD), ultraviolet-visible spectroscopy (UV-Vis), and Fourier transform infrared spectroscopy (FTIR). The in vitro cytotoxicity of green synthesized CeO₂ was assessed against cervical cancerous cells (HeLa). The exposure of CeO₂ to HeLa cells at 10–125 µg/mL caused a loss in cellular viability against cervical cancerous cells in a dose-dependent manner. The antibacterial activity of the CeO₂ was assessed against *S. aureus* and *K. pneumonia*. A significant improvement in wound-healing progression was observed when cerium oxide nanoparticles were incorporated into the chitosan hydrogel membrane as a wound dressing.

Keywords: green synthesis; nanobiotechnology; antibacterial activity; wound healing; antioxidant

1. Introduction

Nanobiotechnology is an advanced and emerging field of science and technology consist of metals and metal oxides at the nano range. In addition, nanobiotechnology has many applications, especially in the biomedical field [1–3]. CeO₂ nanoparticles (NPs) have attained significant consideration in nanomedicine because of their promising applications in drug delivery, catalysis, biosensing, and medicine. CeO₂ nanoparticles are relatively stable, have exceptional biocompatibility with little or no toxicity, low cost, and are environmentally friendly [4]. Cerium has two oxidation states, e.g., tetravalent (Ce⁴⁺) and trivalent (Ce³⁺). Therefore, cerium oxide exists as two different oxides ((i.e., Ce₂O₃ (Ce³⁺) and CeO₂ (Ce⁴⁺)) depending on the nature of the materials [4,5]. CeO₂ NPs have a cubic fluorite structure, and Ce³⁺ and Ce⁴⁺ co-occur on their surface.

The major benefit of cerium dioxide is to produce an oxygen vacancy in the lattice [6,7]. Therefore, the redox properties of CeO₂ NPs have been improved and are helpful for various diseases associated with oxidative stress problems. Moreover, cerium oxide nanopar-

ticles can produce several reactive oxygen species (ROS) that are crucial for in vitro activities [8,9]. Wound healing is the main part of the inflammatory progression that is composed of several physical procedures that depend on the corresponding functions of vascular endothelial growth factor (VEGF). The integrity of the skin can be restored by the healing of wounds caused by incision or accidental injuries [10,11]. Numerous factors, such as diabetes, can delay the process of wound healing, which slows down the blood flow and angiogenesis process at the wound site [12]. Currently, a polymer-based wound dressing impregnated with metal oxide nanoparticles has been used to treat various types of wounds. ROS produced by the metal oxide nanoparticles stimulate the angiogenesis process [12–14].

Abelmoschus esculentus has been used for quite a while as a consumable vegetable in various countries. It contains proteins, enzymes, vitamins, and carbohydrates. *Abelmoschus esculentus* exhibits anticancer, antidiabetic, and antifungal activities, owing to its high free radical antioxidant activity [15,16]. *Abelmoschus esculentus* is an excellent source of flavonoids and polysaccharides and is associated with immune system modulation. Numerous studies have indicated that the biomolecules in the *Abelmoschus esculentus* (okra) extract (e.g., terpenoids, alkaloids, tannins, and flavonoids) are essential in the abatement of metals ions and eventual stabilization of nanoparticles [17].

Various studies have been reported chemical and physical approaches for preparing metal and metal oxide nanoparticles in a very short period of time. In chemicals synthesis methods, a toxic material can be adsorbed at the surface of nanoparticles that may cause adverse effects in a biological environment [18,19]. Currently, plant-mediated preparation of metallic nanoparticles is gaining importance because the preparation is simple and eco-friendly, and the extract of these plants consists of different biomolecules such as vitamins, proteins, surfactants, and carbohydrates, which help to stabilize the nanoparticles [20,21]. Therefore, in this study, CeO₂ nanoparticles were prepared by green synthesis using the *Abelmoschus esculentus* extract. The components existing in the *Abelmoschus esculentus* extract are used as effective capping and reducing agents. Moreover, this study evaluated the cytotoxicity of CeO₂ NPs on cervical cancerous cells and showed extensive antioxidant activity. In addition, this study aimed to investigate the healing response on a cutaneous wound using green synthesized CeO₂ nanoparticles incorporated with chitosan hydrogel membrane.

2. Materials and Methods

2.1. Materials

Chitosan (degree of deacetylation: 85%), cerium nitrate hexahydrate (Ce(NO₃)₃·6H₂O), ethanol (C₂H₅OH), glycerol, 2,2-diphenyl-1-picrylhydrazyl (DPPH), acetic acid (CH₃COOH), and sodium hydroxide (NaOH) were purchased from Sigma Aldrich (Schnelldorf, Germany). Deionized and distilled water were used throughout the experiment. The bacterial strains of *S. aureus* and *K. pneumonia* were obtained from The Islamia University of the Bahawalpur, Bahawalpur, Pakistan.

2.2. Green Synthesis of CeO₂ Nanoparticles

Fresh fruits of *Abelmoschus esculentus* (okra) were obtained, thoroughly washed with running tap water, and then cut into small parts. Then, 20 g of okra fruit pieces were immersed in 150 mL of distilled water overnight at room temperature. Then, the okra fruit solution was extracted using a Whatman No.1 filter paper. Afterward, a 0.5 M solution of cerium nitrate hexahydrate [Ce(NO₃)₃·6H₂O] was prepared in deionized water, and a further 10 mL of the okra extract was mixed up into the precursor solution. At that time, a prepared 2 M sodium hydroxide (NaOH) solution was added to the mixture dropwise. Then, the solution was centrifuged and washed with distilled water three times and then ethanol. Furthermore, the obtained precipitates were dried at 120 °C for 6 h, calcinated for 4 h at 600 °C to evaporate water, and powdered by mortar and pestle to obtain a fine powder consisting of a CeO₂ NPs-mediated okra extract.

2.3. Characterization

The characterization of CeO₂ NPs provides a complete assessment of the morphology, crystalline size, stability, and most importantly functional groups liable to the bioreduction of the synthesized nanoparticles. The CeO₂ NP, CS-CeO₂ nanocomposite morphology was observed by SEM (JEOL, JSM-6480, Tokyo, Japan). The X-ray diffraction of CeO₂ NPs was performed on PANalyticalX'Pert-PRO and interpreted using a matching software. A UV-visible spectrophotometer (Shimadzu, UV-2450, Tokyo, Japan) was utilized to acquire the absorption spectra of CeO₂ NPs. CeO₂ nanoparticles were also evaluated for the existence of biomolecules by Fourier transform infrared spectroscopy (FTIR, Thermo Fischer Scientific, Waltham, MA, USA).

2.4. Antioxidant Activity

Briefly, various concentrations of CeO₂ NPs (20, 40, 60, 80 and 100 µg/mL) were added to 10 mL of a 0.1 mM 2,2-diphenyl-1-picrylhydrazyl (DPPH) solution and kept in complete darkness for at least 40 min at room temperature. Absorbance was recorded using ethanol as black at 517 nm wavelength. Ascorbic acid was used as the standard in all performing experiments. The antioxidant activity of green synthesized CeO₂ NPs was evaluated by DPPH radical scavenging assay using the following formula [22]:

$$\% \text{ Inhibition} = \frac{\text{Absorbance of Control} - \text{Absorbance of Sample}}{\text{Absorbance of Control}} \times 100$$

2.5. Cell Culturing and Exposure with CeO₂ Nanoparticles

A T75 flask was used to culture HeLa cell lines. Hanks salt (10%) was supplemented with MEM (minimum essential medium), fetal bovine serum (FBS, 10 mL) and glutamine (2 mL). Moreover, the cells were incubated for 24 h at 37 °C to attain well interaction with the substratum. The cells were further sub-cultured once or twice every week. Then, the cells were composed using trypsin when the 75–85% convergence was obtained [23,24]. Furthermore, CeO₂ NPs at the concentrations of 25–100 µg/mL was added for 24 h at 37 °C to the solution containing 5% carbon dioxide and 10% fetal bovine serum.

2.6. In Vitro Measurement of Cellular Cytotoxicity (MTT Assay)

Human cervical carcinoma HeLa cells were added to a 96-well plate and then incubated in 5% CO₂ at 37 °C. Then, treated and untreated cells were exposed to increasing concentrations of CeO₂ ranging from 10 to 125 µg/mL and allowed to incubate for 24 h. The MTT assay was controlled in each well; a total of 30 µL of MTT (20 mg/mL) was mixed and incubated for 4 h. Then, the medium was removed, and the cells were mixed in 100 µL of the DMSO solvent [24,25]. A microplate reader was used to measure the absorbance of the samples at 595 nm wavelength.

2.7. HeLa Cells Morphological Analysis

HeLa cells were put into a six-well plate. Each well contained 1×10^4 cells and was treated with CeO₂ NPs synthesized by the green extraction method with increasing concentrations for 12 h. The variation in the morphology of HeLa cells induced by CeO₂ NPs were observed using 20× magnified inverted phase-contrast microscopy [23].

2.8. Antibacterial Study

The agar-well diffusion process was followed to analyze the bactericidal potential of green synthesized CeO₂ NPs counter to *S. aureus* (Gram-positive) and *K. pneumonia* (Gram-negative) bacterial strains. First, the nutrient agar plates were prepared using 38 g of agar powder dissolved in 1 L of distilled water; then, the agar solution was autoclaved at 121 °C for 20 min. Then, it was cooled, mixed well, and poured into Petri plates (20 mL/plate); then, the agar plates were swabbed with bacterial strains [26]. At that time, these wells were exposed to 0.05 mL of the solution containing CeO₂ nanoparticles at various concentrations.

Then, these plates were incubated at 37 °C for 24 h. Then, the antibacterial activities of such nanoparticles were evaluated by measuring the inhibition zone around the wells.

2.9. Chitosan Hydrogel–CeO₂ Composite Membranes Preparation

The chitosan-based hydrogel membranes were prepared by the freeze–gelation process. For this, a 2% solution of chitosan (CS) was prepared into the 1% acetic acid (25 mL). The green synthesized CeO₂ nanoparticles (1% w.r.t chitosan) were suspended in deionized water via sonication for 5 min; then, the prepared suspension of CeO₂ NPs was added to the CS solution, and the mixture solution was kept under continuous stirring for 2 h. Then, the glycerol (3 mL) was added up as a crosslinking material for CS, and the solution was kept in an oven at 80 °C for 4 h. After that, the homogeneous solution was cooled to normal temperature, poured into the Petri plate, and frozen at –20 °C for 2 days. Then, 3 M NaOH solution in ethanol was chilled at –20 °C, poured onto the Petri plate of frozen chitosan, and frozen at –20 °C for 24 h. The prepared hydrogel was washed with ethanol (50%) three times and then distilled water until the neutralization (pH = 7) of the membrane. The same process was followed for the preparation of chitosan and 5% CeO₂ NPs hydrogel membrane as dressings for wound treatment.

2.10. Wound-Healing Activity

2.10.1. Swelling Percent of Chitosan Hydrogel–CeO₂ Membranes

The membranes were cut into small and equal (1 cm × 1 cm) pieces for each sample in triplicate. The cut pieces were immersed in 4 mL of phosphate buffer saline (PBS) solution. The samples were taken out at a specific time interval (0.5 h, 2 h, 4 h, 8 h, 16 h, 24 h) and immediately weighed. The swelling percent of the membranes was evaluated by using the following formula:

$$\text{Swelling \%} = \frac{W_2 - W_1}{W_1} \times 100.$$

In expression, W₁ represents the dry weight of the sample before immersion in solution and W₂ represents the weight after immersion [27].

2.10.2. Animal Trial

Male albino rats (9–10 weeks old and weighing approximately 220–250 g) were purchased. All animals were sustained at room temperature and given free access to water and food. All rat skin incision trials were conducted at Islamia University Bahawalpur with animal ethics committee number PAEC/21/45. All rats were divided into three groups, each group containing 4 rats randomly. Group one was treated with chitosan hydrogel membrane considered as the control group, group two was treated with chitosan hydrogel membrane loaded with 1% cerium nanoparticles, and group three was treated with 5% cerium oxide nanoparticles to evaluate the impact of green synthesized CeO₂ NPs. All rats were anesthetized, and 2 cm full-thickness skin excision wounds were made. The prepared nanoparticles were locally applied at the wound place every day depending on the selected group. Finally, the wound diameter was measured every day [28].

2.11. Statistical Analysis

The outcomes were assessed as the mean ± standard deviation of 3 experiments. The data were assessed by Student's *t*-test, and the values of *p* < 0.05 measured using the Excel software were statistically significant.

3. Results and Discussion

3.1. X-Ray Diffraction Analysis

The XRD result of green synthesized CeO₂ nanoparticles is shown in Figure 1. A strong and sharp diffraction peak revealed the crystalline nature of CeO₂ nanoparticles. The indexed diffraction peaks at the 2θ position of 28.43°, 33.62°, 48.38°, 57.74°, 59.03°, 69.37°, 76.69°, and 79.09°, corresponding to (111), (200), (220), (311), (222), (400), (331),

and (420) crystal planes agreed with the COD library with the card no 96-900-9009 [29]. The XRD planes show the cubic structure for cerium dioxide nanoparticles with the lattice constant (a) value is 5.435 Å. The unit volume for green synthesized CeO₂ mediated with *Abelmoschus esculentus* is calculated to be 160.54 Å³.

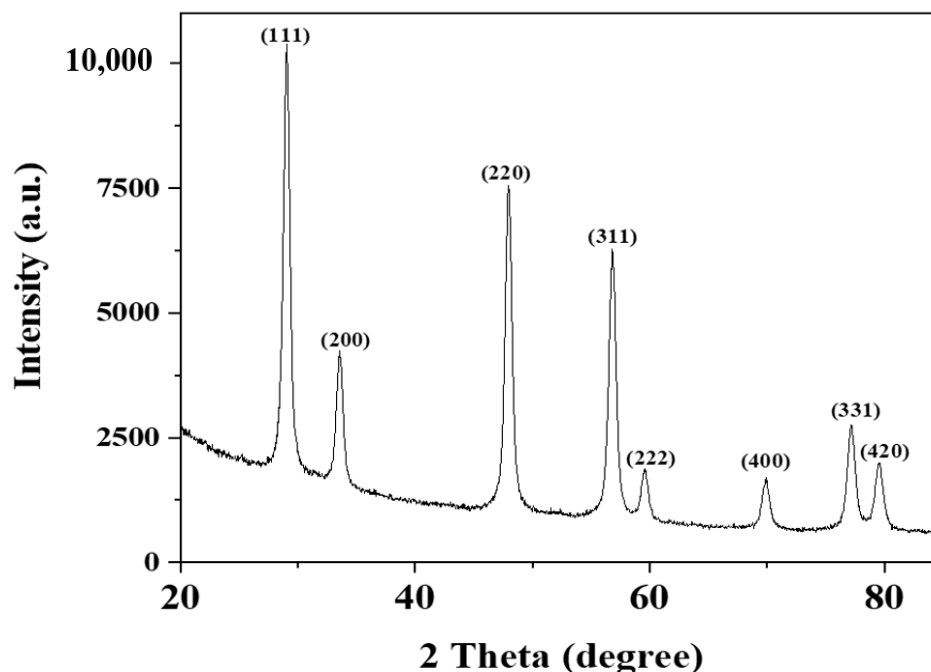


Figure 1. XRD patterns of CeO₂ nanoparticles.

The crystallite size of the synthesized nanoparticles is calculated the Debye–Scherrer formula:

$$\text{Average Crystallite Size } (D) = \frac{0.9\lambda}{\beta \cos\theta}$$

In the formula, λ is the wavelength of the used X-ray for the analysis, β is the angular peak width at half maxima with units in radian, and θ represents the Bragg's diffraction angle. The average crystallite size was approximately 30 nm using the above-mentioned mathematical relation.

3.2. SEM Analysis

The SEM analysis of the prepared CeO₂ nanoparticles using the *Abelmoschus esculentus* extract is shown in Figure 2a. The morphological observations revealed that green synthesized CeO₂ NPs were fully homogenous. The average diameter of CeO₂ NPs was calculated 36 nm by PSD analysis, as shown in Figure 2b using the Image J software. The particle size was approximately 35–40 nm, which almost confirmed the crystallite size determined by Scherer's formula in XRD analysis [30,31].

Furthermore, SEM was utilized to investigate the surface morphology of the prepared chitosan (CS), CS-1% CeO₂, and CS-5% CeO₂ hydrogel membranes, as shown in Figure 2c,d. These SEM images exhibited the porous surface of the chitosan-based hydrogel membranes, these pores are interconnected to each other, and the nanoparticles are homogeneously distributed on the exterior of the hydrogel membranes.

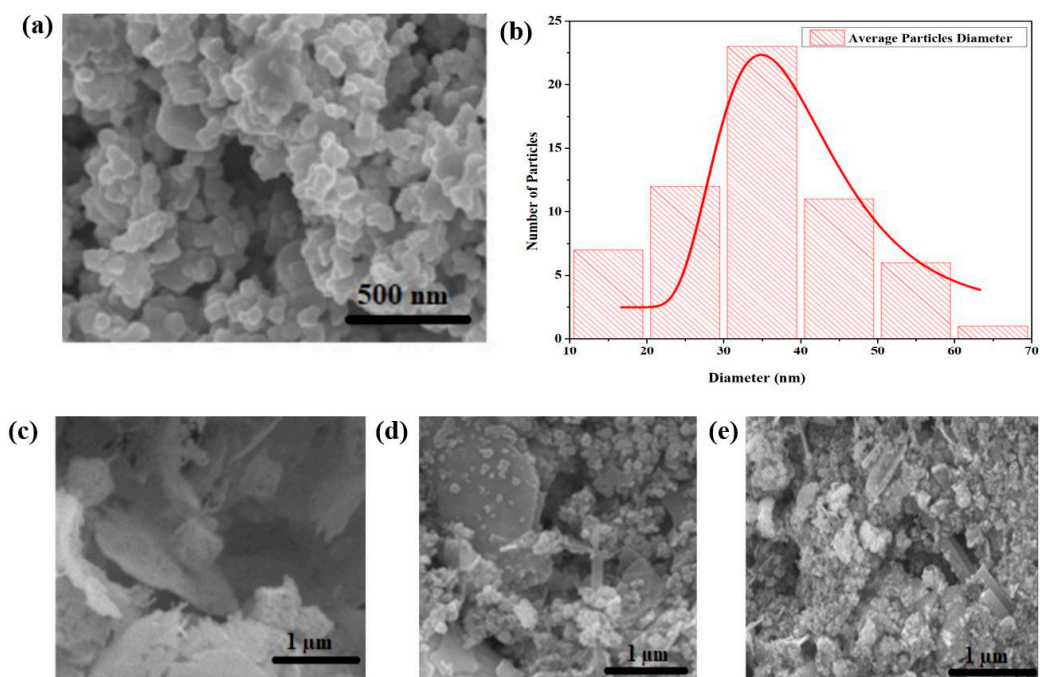


Figure 2. Surface morphology analysis by SEM: (a) green synthesized CeO₂ NPs, (b) PSD analysis of CeO₂ nanoparticles, (c) chitosan hydrogel membrane, (d) chitosan-loaded 1% CeO₂ NPs; (e) chitosan-loaded 5% CeO₂ NPs.

3.3. UV-Visible Analysis

The absorption spectrum of green synthesized CeO₂ NPs measured by UV-vis spectroscopy is shown in Figure 3a. The maximum absorption band is located at 350 nm, which indicates the development of CeO₂ nanoparticles. The presence of an expansion band also indicates the presence of oxidizing polyphenols, which are important for preventing the agglomeration of CeO₂ nanoparticles [31].

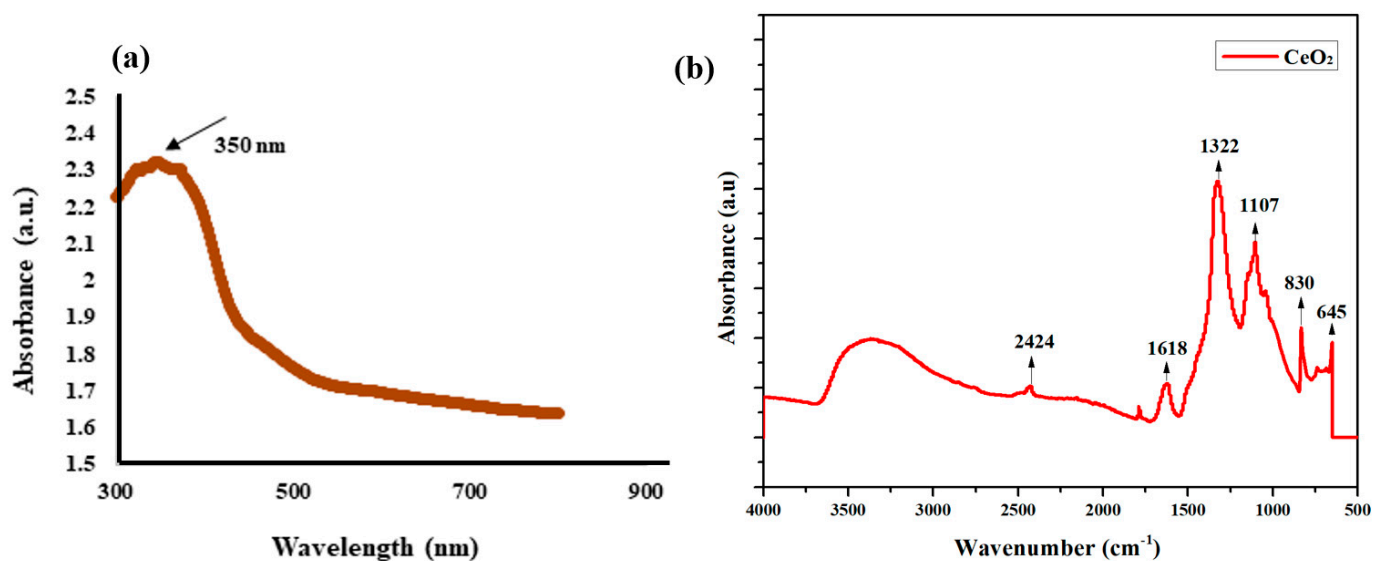


Figure 3. Green synthesized CeO₂ nanoparticles (a) UV-visible and (b) FTIR spectroscopy.

3.4. FT-IR Analysis

Figure 3b shows the FTIR results, which indicate that the stabilization of CeO₂ NPs is due to the presence of phenolic and flavonoids compounds in the *Abelmoschus esculentus*

extract. The peaks, which appeared at 3200–3500 cm^{-1} , revealed the presence of the hydroxyl group (O-H) stretching frequency. The band at 645 cm^{-1} was ascribed to the Ce-O vibrations of green synthesized CeO_2 NPs. The presence of minor distortions at 2424 cm^{-1} range indicates the presence of NH bonds in the *Abelmoschus esculentus* extract. The stretching vibration at 1322 cm^{-1} indicates the existence of the C–C bond, which implies the presence of polyphenol groups owing to the extract. In addition, the peak at 1618 cm^{-1} could be corresponded to the H-O-H group [32–35].

3.5. Antioxidant Activity of Green Synthesized CeO_2 NPs Mediated *Abelmoschus Esculentus*

In this study, the antioxidant activity of CeO_2 NPs was highly dependent on the gradual increase in the concentration from 20 to 100 $\mu\text{g}/\text{mL}$ of nanoparticles, as shown in Figure 4. For CeO_2 , the DPPH radical scavenging values were obtained (51.32%, 62.02%, 72.13%, 83.21%, and 88.15%) with the gradual increase in concentration of CeO_2 nanoparticles. The investigations showed that CeO_2 NPs mediated by the *Abelmoschus esculentus* extract showed better antioxidant properties than ascorbic acid. The ascorbic acid was used as the control to compare the antioxidant properties [36]. The antioxidant activity can be related to the transfer of electrons from oxygen atoms on the particle surface to the nitrogen atom of DPPH molecules, and DPPH forms stable molecules by accepting the electron. The IC_{50} values for ascorbic acid and CeO_2 NPs were observed at 9.36 $\mu\text{g}/\text{mL}$ and 15.47 $\mu\text{g}/\text{mL}$, respectively. Previous studies have shown that many metal nanoparticles can act as antioxidants and scavengers to free radicals [37]. It is also described that the antioxidant activity occurs mostly because of the high surface to volume ratio of the nanostructures. Correspondingly, zinc oxide NPs have greater scavenging action at higher concentrations [38]. However, recent results indicate that CeO_2 NPs are excellent candidates as antioxidants.

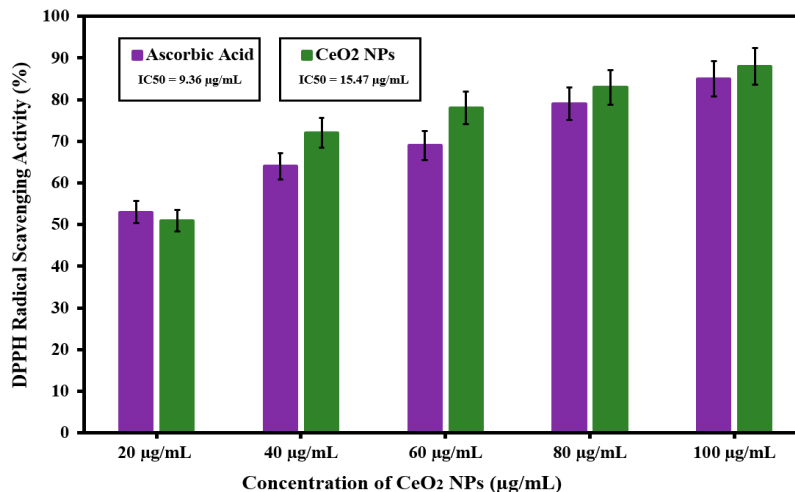


Figure 4. DPPH radical scavenging action of CeO_2 nanoparticles and ascorbic acid.

3.6. Evaluation of Anticancer Activity of Green Synthesized CeO_2 NPs Mediated *Abelmoschus Esculentus*

HeLa cells were used to assess the cytotoxicity of CeO_2 NPs using *abelmoschus esculentus* as a capping agent in the green synthesis method, and the MTT assay was used at different doses for 24 h. Figure 5a shows that the cell viability of 93%, 75%, 66%, 55%, 43%, and 33% decreased when HeLa cells were exposed to green synthesized CeO_2 at increasing concentrations (10, 25, 50, 75, 100, and 125 $\mu\text{g}/\text{mL}$). The IC_{50} value was observed as 85.74 $\mu\text{g}/\text{mL}$ for the HeLa cells viability.

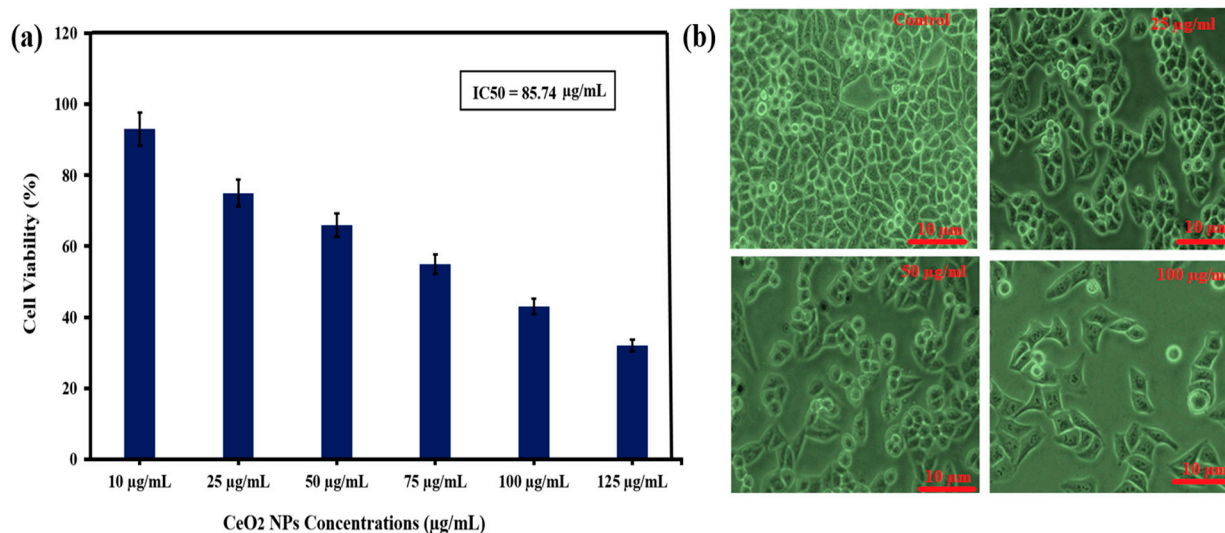


Figure 5. (a) Cell viability (%) of CeO₂ treated HeLa cells after 24 h, (*t*-test). (b) Effect of green synthesized CeO₂ NPs on HeLa cells at different doses (25, 75, and 100 µg/mL) and untreated cells (control).

In addition, CeO₂ NPs using the *Prosopis farcta* extract confirmed the cytotoxicity effects on the HT-29 cell line [39]. It was shown that the number of cells was reduced by employing the biosynthesized cerium oxide nanoparticles using carrageenan, which was highly dependent on the concentration of WEHI 164 malignant cells. In addition, the obtained data coincided with previous data, i.e., the loss in cell viability was dose/concentration-dependent [40–44].

In previous studies, it was suggested that the CeO₂ NPs are toxic to cancerous cells but did not show any toxicity to the normal cells; also, higher concentrations have no toxic effect on the normal cells. A previous study also reported the use of 400 µg/mL CeO₂ concentration for the evaluation of the anticancer effect against the human lungs cancer line. It can be suggested that the CeO₂ NPs toxicity is specified only for cancerous cells and they may be safer for in vivo studies also in medicine and industry [45,46].

Furthermore, both cell morphology and cell viability assay results favored each other to encounter cervical HeLa cells. Figure 5b shows the photomicrograph of HeLa cells after approximately 24 h in the untreated (control) and presence of CeO₂ NPs. In the control sample, the HeLa cells seem to have long-armed blurry cell borders that represent epithelial and bulky cells. In addition, with an increase in the concentration (25, 75, and 100 µg/mL) of green synthesized CeO₂ nanoparticles during cervical HeLa cell treatment, a notable impact is observed compared to the control group. The nanoparticles-treated HeLa cells are considerably less dense and have contracted arms compared to the untreated (control) group, as shown in Figure 5b.

At lower concentrations (25 µg/mL), the cells started to shrink, and similarly, as the concentration increases (75 µg/mL), the further morphological changes could be seen, which indicate the apoptosis of cells. At 100 µg/mL, more apoptosis of the cancerous cells was observed. A similar pattern of anticancer was also observed for green synthesized CeO₂ using orange peel extract [47].

3.7. Antibacterial Activity of Green Synthesized CeO₂ NPs Mediated *Abelmoschus Esculentus*

The antibacterial activity potential of green synthesized CeO₂ NPs was tested against two pathogenic bacterial strains of *S. aureus* and *K. pneumonia* using the agar well diffusion method. The inhibition zones indicated the antibacterial effect of CeO₂ nanoparticles at different concentrations. It was observed that the impact of increasing the concentration of CeO₂ nanoparticles increased the inhibition of bacteria. Among three concentrations (10, 20, and 30 µg/mL), the 30 µg/mL of CeO₂ nanoparticle concentration showed a higher inhibition zone against *S. aureus* (21 mm), which is Gram-positive, and *K. pneumonia*

(19 mm), which is Gram-positive. Based on the results obtained by the agar well diffusion method, it is proposed that with an increase in the concentration of nanoparticles, the inhibition zone was increased at different concentrated doses for *S. aureus* and *K. pneumoniae* strains, as shown in Figure 6a,b. This study shows that the antibacterial results of CeO₂ NPs-mediated *abelmoschus esculentus* are vastly dependent on the concentration of nanoparticles; as the concentration was increased, the zone of inhibition also increased. From antibacterial study, it is seen that *S. aureus* (Gram-positive) bacteria are relatively more susceptible to CeO₂ NPs than the *K. pneumoniae* (Gram-negative) bacteria. It could be suggested that the Gram-positive bacteria are more sensitive to the reactive oxygen species (ROS), and this might be the reason of a higher zone of inhibition in the *S. aureus* bacterial strains. To compare our results, the same trend was also reported in green synthesized CeO₂ mediated *Gloriosa Superba* leaves extract regarding the higher inhibition zone of Gram-positive bacterial strains [32].

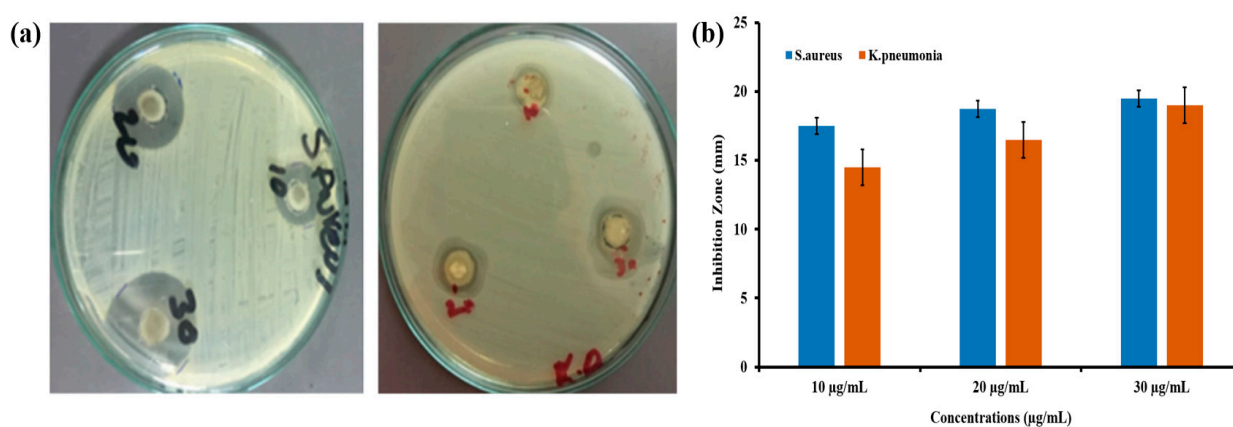


Figure 6. (a) Clear inhibition zone formed by synthesized CeO₂ NPs using the *Abelmoschus Esculentus* extract against *S. aureus* and *K. pneumoniae*. (b) Histogram representation for all measured inhibition zones at different concentrations of CeO₂ NPs.

The CeO₂ potential against the microorganism greatly depends upon the greater surface to volume ratio, which causes the better interaction of nanoparticles with the surface of bacteria. In this study, we have synthesized nanoparticles with spherical morphology and excellent average diameter which, as discussed in SEM analysis, is highly correlated with the antibacterial potential. Moreover, the positive surface of the nanoparticle ions and negatively charged surface of the bacteria causes a strong electrostatic interaction, which ruptures the outer surface of the bacteria and causes cell death.

The basic mechanism of the antibacterial activity of the CeO₂ NPs is that when the light falls on the nanoparticle surfaces, they absorb the photo-energy greater than the CeO₂ bandgap. Then, the electrons (e⁻) move from the valence band to the conduction band, and holes (h⁺) are generated in the valence band. The photo-generated electrons and holes cause reduction and oxidation processes. The electron reacts with oxygen and produces the superoxide anion (O₂^{•-}), and this is known as the reduction process. Furthermore, the holes react with the hydroxyl ions and produce the hydroxyl radical (•OH) by the oxidation process. Hydroxyl radicals are a very reactive oxidant to the organic biomolecules such as DNA nucleic acid, proteins, and lipids. The interaction of superoxide anions in water contents produces indirectly singlet oxygen (¹O₂), which is the main mediator of the phototoxicity caused by the damage of treated tissues. These photo-generated hydroxyl radicals such as superoxide anion and singlet oxygen known as the reactive oxygen species (ROS) which reach through their direct interaction with the cell wall and penetration to the internal part of the bacteria destroy the DNA, proteins, and lipids functions, leading to the death of bacterial cells. In addition, the mechanical damage by the direct interaction of the CeO₂ NPs with the bacterial surface causes the denaturing [48].

3.8. Wound-Healing Potential of Green Synthesized CeO₂ NPs Mediated *Abelmoschus Esculentus*

3.8.1. Swelling Studies of Hydrogel Membrane

Fluid such as plasma or serum from the wound absorbed by the dressing has a key role in wound healing. So, it is important to know about the swelling capacity of the prepared hydrogel-based dressings for the wound. Figure 7 represents the time-dependent swelling behavior of the chitosan (control) and chitosan-loaded 1% and 5% green synthesized CeO₂ nanoparticles. The chitosan hydrogel membrane represents the highest swelling capacity. In the other chitosan hydrogel membrane incorporated with CeO₂ NPs, it was evaluated that the swelling capacity of the membrane dressing decreases with the cumulative concentration of the nanoparticles. There was a decrease in the swelling capacity of the membranes due to the higher crosslinking; the higher crosslinking occupies the hydrophilic functional sites available in the hydrogel matrix for intermolecular bonding [49].

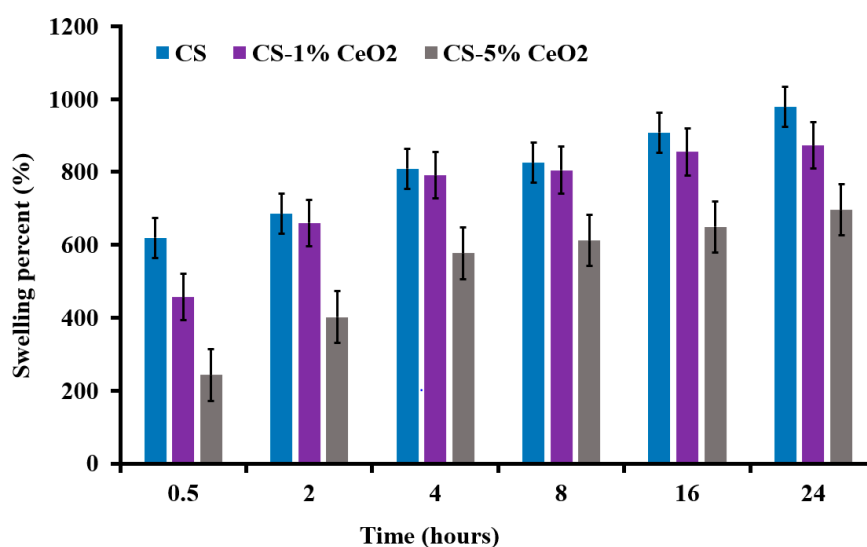


Figure 7. Demonstration of the swelling percent of the chitosan-based hydrogel membranes.

3.8.2. Animal Trials

Figure 8a shows the fine changes in wound extent during the wound-healing development for different samples of green synthesized CeO₂. The healing procedure was assessed by observing regular changes in the color of the wound. The photographs of the representative rat wounds from each group were acquired to evaluate the healing potential of the cerium oxide nanoparticles at different concentrations. After 4 days of healing, fresh skin was grown (after it was treated with 1% and 5% cerium oxide nanoparticles); it had fewer scabs and was smoother than the control group; these observations represent the initiation of the wound-healing process. On day 7, a brown dark color was observed for the cerium oxide nanoparticles-treated groups. These observations confirm the initiation of wound-healing progress by producing collagen. On day 11, the 1% and 5% cerium oxide nanoparticles-treated group showed that the wounds were significantly reduced in size compared to the control group. Regarding the scab formation of the control group, an increase in the concentration of cerium oxide nanoparticles significantly affected the wound size.

The wound closure comparison of incision is shown in Figure 8b, which represents the effect of the concentration of cerium oxide nanoparticles on the diameter of the wound compared with the control sample. On day 15, the wound site differed from the treated group in which the maximum contraction of the wounds was achieved by increasing the concentration of the cerium nanoparticles as compared to the control group, which showed a visibly larger wound size.

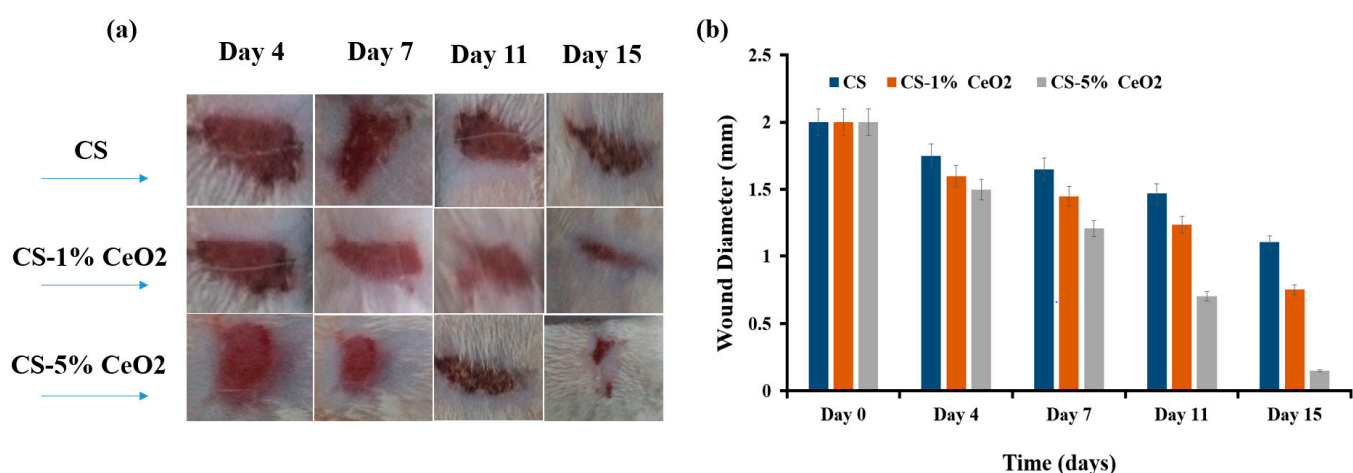


Figure 8. (a) Photographs representing the analysis of incision wound treatment with green synthesized CS-1% CeO₂ and CS-5% CeO₂ nanoparticles incorporated in chitosan hydrogel membrane groups. (b) Comparison of wound reduction in diameter.

According to these observations, it can be concluded that CS-1% CeO₂ and CS-5% CeO₂ nanoparticles incorporated in chitosan hydrogel membrane groups stimulate the wound-healing process specifically during the initial stages. In the wound-healing experiment in vivo, the groups treated with cerium oxide nanoparticles incorporated in chitosan hydrogel membrane showed better wound healing after 11 days of excision. As discussed above, green synthesized cerium oxide nanoparticles have exceptional antibacterial properties, which considerably affect the wound-healing process. Recent studies have also reported that metal oxide nanoparticles reduce bacterial contamination, increase collagen formation and tensile strength, and decrease wound inflammation. In addition, the increasing concentration of nanoparticles affected the regulation of fibrogenic cytokines, which greatly contributed to the healing process [50].

4. Conclusions

Cerium oxide nanoparticles were green synthesized and characterized by manifold techniques (UV-visible spectroscopy, SEM, XRD, and FTIR). Furthermore, CeO₂ NPs have resilient antioxidant activity, while MTT assay outcomes and morphological analysis after 24 h indicated that CeO₂ NPs demonstrated a clear cytotoxic effect against HeLa cell lines. CeO₂ NPs were considered to be associated with a cell-killing mechanism when used at higher doses (50–125 µg/mL). The green synthesized cerium oxide nanoparticles showed higher antioxidant activities and bactericidal effect against both Gram-positive and Gram-negative strains. The in vivo studies on rats confirmed that green synthesized cerium oxide nanoparticles appeared to be effective for skin wound treatment. The wound treatment with cerium nanoparticles induced collagen deposition and increased the tensile strength of skin as compared to the control group. This study may serve as a fruitful platform to explore the green synthesis of nanoparticles in various biomedical therapeutics.

Author Contributions: H.E.A., Y.I., M.H.A. and M.A. wrote the paper while Z.B., A.H., N.Y., W.A.F., and S.A. analyzed the data A.F. and H.A. contributed significantly in arranging the manuscript. All authors have read and agreed to the published version of the manuscript.

Funding: This research received no external funding.

Institutional Review Board Statement: Wound healing analysis was done via PAEC/21/45.

Informed Consent Statement: Experiment was evaluated on rats via PAEC/21/45.

Data Availability Statement: All relevant data are included in the article.

Acknowledgments: Researchers Supporting Project number (RSP-2021/397), King Saud University, Riyadh, Saudi Arabia.

Conflicts of Interest: The authors declare no conflict of interest.

Sample Availability: Samples of the compounds are available from the authors.

References

1. Singh, J.; Dutta, T.; Kim, K.H.; Rawat, M.; Samddar, P.; Kumar, P. 'Green' synthesis of metals and their oxide nanoparticles: Applications for environmental remediation. *J. Nanobiotechnol.* **2018**, *16*, 84. [\[CrossRef\]](#)
2. Makarov, V.V.; Love, A.J.; Sinityna, O.V.; Makarova, S.S.; Yaminsky, I.V.; Taliensky, M.E.; Kalinina, N.O. "Green" nanotechnologies: Synthesis of metal nanoparticles using plants. *Acta Nat.* **2014**, *6*, 20. [\[CrossRef\]](#)
3. Yadi, M.; Mostafavi, E.; Saleh, B.; Davaran, S.; Aliyeva, I.; Khalilov, R.; Nikzamir, M.; Nikzamir, N.; Akbarzadeh, A.; Panahi, Y.; et al. Current developments in green synthesis of metallic nanoparticles using plant extracts: A review. *Artif. Cells Nanomed. Biotechnol.* **2018**, *46*, 336–343. [\[CrossRef\]](#) [\[PubMed\]](#)
4. Deshpande, S.; Patil, S.; Kuchibhatla, S.V.; Seal, S. Size dependency variation in lattice parameter and valency states in nanocrystalline cerium oxide. *Appl. Phys. Lett.* **2005**, *87*, 133. [\[CrossRef\]](#)
5. Das, S.; Dowding, J.M.; Klump, K.E.; McGinnis, J.F.; Self, W.; Seal, S. Cerium oxide nanoparticles: Applications and prospects in nanomedicine. *Nanomedicine* **2013**, *8*, 1483–1508. [\[CrossRef\]](#)
6. Xu, C.; Qu, X. Cerium oxide nanoparticle: A remarkably versatile rare earth nanomaterial for biological applications. *NPG Asia Mater.* **2014**, *6*, e90. [\[CrossRef\]](#)
7. Beaudoux, X.; Virost, M.; Chave, T.; Durand, G.; Leturcq, G.; Nikitenko, S.I. Vitamin C boosts ceria-based catalyst recycling. *Green Chem.* **2016**, *18*, 3656–3668. [\[CrossRef\]](#)
8. Aalapathi, S.; Ganapathy, S.; Manapuram, S.; Anumolu, G.; Prakya, B.M. Toxicity and bio-accumulation of inhaled cerium oxide nanoparticles in CD1 mice. *Nanotoxicology* **2014**, *8*, 786–798. [\[CrossRef\]](#)
9. Maqbool, Q. Green-synthesised cerium oxide nanostructures (CeO₂-NS) show excellent biocompatibility for phyto-cultures as compared to silver nanostructures (Ag-NS). *RSC Adv.* **2017**, *7*, 56575–56585. [\[CrossRef\]](#)
10. Eming, S.A.; Martin, P.; Tomic-Canic, M. Wound repair and regeneration: Mechanisms, signaling, and translation. *Sci. Transl. Med.* **2014**, *6*, 265. [\[CrossRef\]](#) [\[PubMed\]](#)
11. Delavary, B.M.; van der Veer, W.M.; van Egmond, M.; Niessen, F.B.; Beelen, R.H. Macrophages in skin injury and repair. *Immunobiology* **2011**, *216*, 753–762. [\[CrossRef\]](#)
12. Demidova-Rice, T.N.; Durham, J.T.; Herman, I.M. Wound healing angiogenesis: Innovations and challenges in acute and chronic wound healing. *Adv. Wound Care* **2012**, *1*, 17–22. [\[CrossRef\]](#)
13. Mohammadinejad, R.; Karimi, S.; Irvani, S.; Varma, R.S. Plant-derived nanostructures: Types and applications. *Green Chem.* **2016**, *18*, 20–52. [\[CrossRef\]](#)
14. El Shafey, A.M. Green synthesis of metal and metal oxide nanoparticles from plant leaf extracts and their applications: A review. *Green Process. Synth.* **2020**, *9*, 304–339. [\[CrossRef\]](#)
15. Ahmed, B.T.; Kumar, S.A. Antioxidant and Antidiabetic properties of *Abelmoschus esculentus* extract—an in vitro assay. *Res. J. Biotechnol.* **2016**, *11*, 34–41.
16. Arapitsas, P. Identification and quantification of polyphenolic compounds from okra seeds and skins. *Food Chem.* **2008**, *110*, 1041–1045. [\[CrossRef\]](#) [\[PubMed\]](#)
17. Xia, F.; Zhong, Y.; Li, M.; Chang, Q.; Liao, Y.; Liu, X.; Pan, R. Antioxidant and anti-fatigue constituents of okra. *Nutrients* **2015**, *7*, 8846–8858. [\[CrossRef\]](#) [\[PubMed\]](#)
18. Rajput, N. Methods of preparation of nanoparticles—a review. *Int. J. Adv. Eng. Technol.* **2015**, *7*, 1806.
19. Fabiano, B.; Reverberi, A.P.; Varbanov, P.S. Safety opportunities for the synthesis of metal nanoparticles and short-cut approach to workplace risk evaluation. *J. Clean. Prod.* **2019**, *209*, 297–308. [\[CrossRef\]](#)
20. Duan, H.; Wang, D.; Li, Y. Green chemistry for nanoparticle synthesis. *Chem. Soc. Rev.* **2015**, *44*, 5778–5792. [\[CrossRef\]](#)
21. Ahmed, S.; Chaudhry, S.A.; Ikram, S. A review on biogenic synthesis of ZnO nanoparticles using plant extracts and microbes: A prospect towards green chemistry. *J. Photochem. Photobiol. B Biol.* **2017**, *166*, 272–284. [\[CrossRef\]](#)
22. Das, D.; Nath, B.C.; Phukon, P.; Dolui, S.K. Synthesis and evaluation of antioxidant and antibacterial behavior of CuO nanoparticles. *Colloids Surf. B Biointerfaces* **2013**, *101*, 430–433. [\[CrossRef\]](#) [\[PubMed\]](#)
23. Fakhar-e-Alam, M.; Rahim, S.; Atif, M.; Aziz, M.H.; Malick, M.I.; Zaidi, S.S.Z.; Suleman, R.; Majid, A. ZnO nanoparticles as drug delivery agent for photodynamic therapy. *Laser Phys. Lett.* **2013**, *11*, 25601. [\[CrossRef\]](#)
24. AlSalhi, M.S.; Aziz, M.H.; Atif, M.; Fatima, M.; Shaheen, F.; Devanesan, S.; Farooq, W.A. Synthesis of NiO nanoparticles and their evaluation for photodynamic therapy against HeLa cancer cells. *J. King Saud Univ. -Sci.* **2020**, *32*, 1395–1402. [\[CrossRef\]](#)
25. Van Meerloo, J.; Kaspers, G.J.; Cloos, J. Cell sensitivity assays: The MTT assay. In *Cancer Cell Culture*; Humana Press: Totowa, NJ, USA, 2011; pp. 237–245.
26. Gurunathan, S. Biologically synthesized silver nanoparticles enhances antibiotic activity against Gram-negative bacteria. *J. Ind. Eng. Chem.* **2015**, *29*, 217–226. [\[CrossRef\]](#)
27. Gotoh, T.; Nakatani, Y.; Sakohara, S. Novel synthesis of thermosensitive porous hydrogels. *J. Appl. Polym. Sci.* **1998**, *69*, 895–906. [\[CrossRef\]](#)
28. Kalantari, K.; Mostafavi, E.; Afifi, A.M.; Izadiyan, Z.; Jahangirian, H.; Rafiee-Moghaddam, R.; Webster, T.J. Wound dressings functionalized with silver nanoparticles: Promises and pitfalls. *Nanoscale* **2020**, *12*, 2268–2291. [\[CrossRef\]](#)

29. Goharshadi, E.K.; Mahvelati, T.; Yazdanbakhsh, M. Influence of preparation methods of microwave, sol–gel, and hydrothermal on structural and optical properties of lanthania nanoparticles. *J. Iran. Chem. Soc.* **2016**, *13*, 65–72. [[CrossRef](#)]
30. Tao, Y.; Gong, F.H.; Wang, H.; Wu, H.P.; Tao, G.L. Microwave-assisted preparation of cerium dioxide nanocubes. *Mater. Chem. Phys.* **2008**, *112*, 973–976. [[CrossRef](#)]
31. Nadeem, M.; Khan, R.; Afridi, K.; Nadhman, A.; Ullah, S.; Faisal, S.; Mabood, Z.U.; Hano, C.; Abbasi, B.H. Green Synthesis of Cerium Oxide Nanoparticles (CeO₂ NPs) and Their Antimicrobial Applications: A Review. *Int. J. Nanomed.* **2020**, *15*, 5951–5961. [[CrossRef](#)]
32. Arumugam, A.; Karthikeyan, C.; Hameed, A.S.H.; Gopinath, K.; Gowri, S.; Karthika, V. Synthesis of cerium oxide nanoparticles using *Gloriosa superba* L. leaf extract and their structural, optical and antibacterial properties. *Mater. Sci. Eng. C* **2015**, *49*, 408–415. [[CrossRef](#)]
33. Kannan, S.K.; Sundrarajan, M. A green approach for the synthesis of a cerium oxide nanoparticle: Characterization and antibacterial activity. *Int. J. Nanosci.* **2014**, *13*, 1450018. [[CrossRef](#)]
34. Fortunati, E.; Puglia, D.; Monti, M.; Santulli, C.; Maniruzzaman, M.; Kenny, J.M. Cellulose nanocrystals extracted from okra fibers in PVA nanocomposites. *J. Appl. Polym. Sci.* **2013**, *128*, 3220–3230. [[CrossRef](#)]
35. Leppänen, K.; Andersson, S.; Torkkeli, M.; Knaapila, M.; Kotelnikova, N.; Serimaa, R. Structure of cellulose and microcrystalline cellulose from various wood species, cotton and flax studied by X-ray scattering. *Cellulose* **2009**, *16*, 999–1015. [[CrossRef](#)]
36. Maryam, S.; Khan, M.R.; Shah, S.A.; Zahra, Z.; Majid, M.; Sajid, M.; Ali, S. In vitro antioxidant efficacy and the therapeutic potential of *Wendlandia heynei* (Schult.) Santapau & Merchant against bisphenol A-induced hepatotoxicity in rats. *Toxicol. Res.* **2018**, *7*, 1173–1190.
37. Kovacic, P.; Somanathan, R. Nanoparticles: Toxicity, radicals, electron transfer, and antioxidants. *Oxidative Stress Nanotechnol.* **2013**, 15–35. [[CrossRef](#)]
38. Zare, M.; Namratha, K.; Byrappa, K.; Surendra, D.M.; Yallappa, S.; Hungund, B. Surfactant assisted solvothermal synthesis of ZnO nanoparticles and study of their antimicrobial and antioxidant properties. *J. Mater. Sci. Technol.* **2018**, *34*, 1035–1043. [[CrossRef](#)]
39. Miri, A.; Sarani, M. Biosynthesis, characterization and cytotoxic activity of CeO₂ nanoparticles. *Ceram. Int.* **2018**, *44*, 12642–12647. [[CrossRef](#)]
40. Nourmohammadi, E.; Oskuee, R.K.; Hasanzadeh, L.; Mohajeri, M.; Hashemzadeh, A.; Rezayi, M.; Darroudi, M. Cytotoxic activity of greener synthesis of cerium oxide nanoparticles using carrageenan towards a WEHI 164 cancer cell line. *Ceram. Int.* **2018**, *44*, 19570–19575. [[CrossRef](#)]
41. Atif, M.; Firdous, S.; Khurshid, A.; Noreen, L.; Zaidi, S.; Ikram, M. In Vitro Study of 5-Aminolevulinic Acid-Based Photodynamic Therapy for Apoptosis in Human Cervical HeLa Cell Line. *Laser Phys. Lett.* **2009**, *6*, 886. [[CrossRef](#)]
42. Atif, M.; Iqbal, S.; Fakhar-e-Alam, M.; Mansoor, Q.; Alimgeer, K.; Fatehmulla, A.; Hanif, A.; Yaqub, N.; Farooq, W.; Ahmad, S. Manganese-Doped Cerium Oxide Nanocomposite as a Therapeutic Agent for MCF-7 Adenocarcinoma Cell Line. *Saudi J. Biol. Sci.* **2021**, *28*, 1233–1238. [[CrossRef](#)] [[PubMed](#)]
43. Atif, M.; Iqbal, S.; Ismail, M.; Mansoor, Q.; Mughal, L.; Aziz, M.H.; Hanif, A.; Farooq, W. Manganese-Doped Cerium Oxide Nanocomposite Induced Photodynamic Therapy in MCF-7 Cancer Cells and Antibacterial Activity. *BioMed Res. Int.* **2019**, *2019*, 7156828. [[CrossRef](#)] [[PubMed](#)]
44. Atif, M.; Fakhar-e-Alam, M.; Firdous, S.; Zaidi, S.; Suleman, R.; Ikram, M. Study of the Efficacy of 5-ALA Mediated Photodynamic Therapy on Human Rhabdomyosarcoma Cell Line (RD). *Laser Phys. Lett.* **2010**, *7*, 757. [[CrossRef](#)]
45. Lord, M.S.; Berret, J.F.; Singh, S.; Vinu, A.; Karakoti, A.S. Redox Active Cerium Oxide Nanoparticles: Current Status and Burning Issues. *arXiv* **2021**, arXiv:2106.06473.
46. Gumustas, M.; Sengel-Turk, C.T.; Gumustas, A.; Ozkan, S.A.; Uslu, B. Effect of polymer-based nanoparticles on the assay of antimicrobial drug delivery systems. *Multifunct. Syst. Comb. Deliv. Biosens. Diagn.* **2017**, 67–108. [[CrossRef](#)]
47. Irshad, M.S.; Aziz, M.H.; Fatima, M.; Rehman, S.U.; Idrees, M.; Rana, S.; Shaheen, F.; Ahmed, A.; Javed, M.Q.; Huang, Q. Green synthesis, cytotoxicity, antioxidant and photocatalytic activity of CeO₂ nanoparticles mediated via orange peel extract (OPE). *Mater. Res. Express* **2019**, *6*, 950. [[CrossRef](#)]
48. Burello, E.; Worth, A.P. A theoretical framework for predicting the oxidative stress potential of oxide nanoparticles. *Nanotoxicology* **2011**, *5*, 228–235. [[CrossRef](#)]
49. Mohandas, A.; Deepthi, S.; Biswas, R.; Jayakumar, R. Chitosan based metallic nanocomposite scaffolds as antimicrobial wound dressings. *Bioact. Mater.* **2018**, *3*, 267–277. [[CrossRef](#)]
50. Zgheib, C.; Hilton, S.A.; Dewberry, L.C.; Hodges, M.M.; Ghatak, S.; Xu, J.; Singh, S.; Roy, S.; Sen, C.K.; Seal, S.; et al. Use of cerium oxide nanoparticles conjugated with microRNA-146a to correct the diabetic wound healing impairment. *J. Am. Coll. Surg.* **2019**, *228*, 107–115. [[CrossRef](#)]